Jørgensen, B.B., D'Hondt, S.L., and Miller, D.J. (Eds.)
Proceedings of the Ocean Drilling Program, Scientific Results Volume 201

18. Data Report: Permeabilities of Eastern Equatorial Pacific and Peru Margin Sediments[1]

Kusali Gamage,[2] Barbara Bekins,[3] and Elizabeth Screaton[2]

ABSTRACT

Constant-flow permeability tests were conducted on core samples from Ocean Drilling Program Leg 201 from the eastern equatorial Pacific and the Peru margin. Eighteen whole-round core samples from Sites 1225, 1226, 1227, 1230, and 1231 were tested for vertical permeabilities. Sites 1225, 1226, and 1231 represent sediments of the open ocean, whereas Sites 1227 and 1230 represent sediments of the ocean margin. Measured vertical permeabilities vary from ~8×10^{-19} m² to ~1×10^{-16} m² for a porosity range of 45%–90%.

INTRODUCTION

Ocean Drilling Program (ODP) Leg 201 was the first ocean expedition that focused on subsurface marine environments to study life in sediments deep beneath the ocean floor (Shipboard Scientific Party, 2003). During Leg 201, seven sites were drilled into a wide range of subsurface environments in both open-ocean and ocean-margin provinces of the eastern tropical Pacific Ocean. These subsurface environments include carbonates and siliceous oozes typical of the equatorial Pacific, clays and nannofossil-rich oozes of the Peru Basin, biogenic and terrigenous-rich sediments of the shallow Peru shelf, and clay-rich deepwater sequences of the Peru slope (Shipboard Scientific Party, 2003).

Fluid flow in sediments can transport nutrients that maintain microbial life in subsurface sediments (Chapelle, 1993); thus, it is important to quantify the rate of fluid flow. Permeability is an important property

[1] Gamage, K., Bekins, B., and Screaton, E., 2005. Data report: Permeabilities of eastern equatorial Pacific and Peru margin sediments. *In* Jørgensen, B.B., D'Hondt, S.L., and Miller, D.J. (Eds.), *Proc. ODP, Sci. Results,* 201, 1–18 [Online]. Available from World Wide Web: <http://www-odp.tamu.edu/publications/201_SR/VOLUME/CHAPTERS/103.PDF>. [Cited YYYY-MM-DD]
[2] Department of Geological Sciences, University of Florida, 241 Williamson Hall, Box 112120, Gainesville FL 32611, USA. Correspondence author: **kusali@ufl.edu**
[3] U.S. Geological Survey, 345 Middlefield Road, Menlo Park CA 94025, USA.

Initial receipt: 2 July 2004
Acceptance: 6 January 2005
Web publication: 11 July 2005
Ms 201SR-103

of the porous medium that controls fluid flow in sediments. In this study, we used core samples from five sites from Leg 201, including open-ocean Sites 1225, 1226, and 1231 and ocean-margin Sites 1227 and 1230 to measure vertical permeabilities (Fig. F1). Each site represents a different subsurface environment. Sites 1225 and 1226 represent the carbonate, siliceous, and chalk sediments of the equatorial Pacific; Site 1227 represents the biogenic oozes and terrigenous sediments of the shallow Peru shelf; Site 1230 represents the hydrate-bearing clays, biogenic oozes, and silt sediments of the lower slope of the Peru trench; and Site 1231 represents deep-sea clays and nannofossil oozes of the Peru Basin (Shipboard Scientific Party, 2003). Constant-flow tests were conducted on core samples to measure the vertical permeability of the sediments.

F1. Locations of drill sites, p. 7.

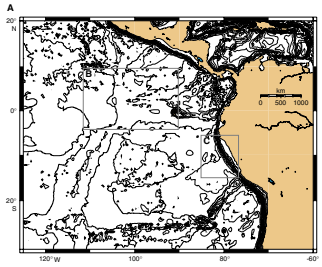

METHODS

The constant-flow approach measures hydraulic gradient while fluid is pumped into and out of the sample. The constant-flow permeability tests were conducted using the Trautwein Soil Testing Equipment Company's DigiFlow K (Figs. F2, F3). The equipment consists of a cell (to contain the sample and provide isostatic effective stress) and three pumps (sample top pump, sample bottom pump, and cell pump). Bladder accumulators allow deionized water in the pumps while an idealized solution of seawater (25 g NaCl and 8 g $MgSO_4$ per liter of water) permeates the sample. ASTM (1990) designation D 5084-90 was used as a guideline for general procedures.

F2. Laboratory setup for vertical permeability testing, p. 9.

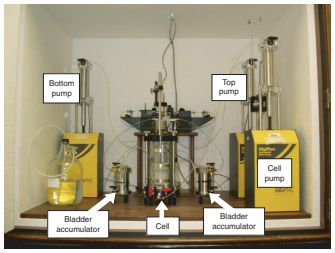

F3. Constant-flow closed system, p. 10.

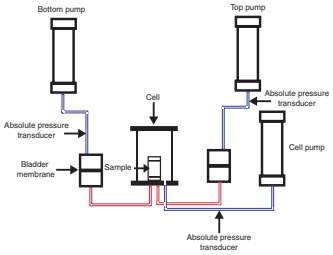

The retrieved Leg 201 core samples were stored in plastic core liners and sealed with wax immediately after sampling to prevent moisture loss. The sealed samples were stored in the refrigerator at 4°C until immediately prior to sample preparation. To provide freshly exposed surfaces, cores were trimmed on both ends immediately before testing using a wire saw or a utility knife, depending on core properties. After trimming the ends of the sample, the diameter and the height of the sample were measured. The Leg 201 samples had a minimum diameter of 2.3 in, and sample heights varied from 2.3 to 3.6 in. The sample was then placed in a flexible-wall membrane and fitted with filter paper and saturated porous disks on both ends. Next, the sample was placed in the cell, which was filled with deionized water so that the membrane-encased sample was completely surrounded by fluid. A small confining pressure of ~0.03 MPa (5 psi) was applied. Flow lines were flushed to remove any trapped air bubbles. After flushing the flow lines, the sample was backpressured at ~0.28 MPa (40 psi) in order to fully saturate the sample. Backpressure was achieved by concurrently ramping the cell pressure and the sample pressure to maintain a steady effective stress of 0.03 MPa. Saturation was verified by measuring the ratio of change in pore water pressure in the porous material to the change in the confining pressure (ASTM, 1990). Once the sample reached saturation, the cell fluid pressure was increased while the sample backpressure was maintained, thus increasing the effective stress on the sample. Once the target effective stress was achieved, cell pressure and backpressure were maintained. The sample was allowed to equilibrate for at least 4 hr and generally overnight (12 hr). Throughout testing, vertical sample displacement and change in cell fluid volume were monitored. The pressure difference between sample top and bottom were measured using a Validyne variable reluctance pressure transducer. The accuracy of the

Validyne variable reluctance pressure transducer was ±5.2 × 10^{-4} MPa (±0.075 psi). All measurements and data were logged digitally in real time.

After the target effective stress level was achieved, a brief constant pressure gradient test was conducted to select an appropriate flow rate for the subsequent constant-flow tests. During the constant-flow tests, flow rates were maintained by the top and bottom pumps, one on each end of the sample, ensuring that the volume of the sample was unchanged. During the permeation step, the head gradient was monitored to ensure that gradients were not excessive (ASTM, 1990). Since fluid pressure in the closed hydraulic system was affected by temperature changes, testing was conducted within a closed cabinet with a fan to keep the internal temperature uniform. The temperature was maintained at ~30ºC (±1°C) during flow tests, and consolidation steps and temperature were monitored throughout the testing phase.

Four to five constant-flow tests were performed at each effective stress level. Once permeability values were obtained, cell pressure was increased and the sample was allowed to equilibrate overnight at the new effective stress. For every sample, four effective stress steps were performed. We used effective stress values ranging from 0.14 to 0.55 MPa. Previous permeability studies (e.g., Bolton and Maltman, 1998; Bolton et al., 2000) have shown that the largest decrease in permeability occurs as effective stress is increased from 0 to 0.1 MPa; subsequently, permeabilities remain relatively constant.

Using these measurements—the specified flow rate, Q (in cubic meters per second), and the pressure difference that was monitored by the testing equipment, hydraulic conductivity, K—values were calculated for each sample using Darcy's Law:

$$Q = -K \times A \times (\mathrm{d}h/\mathrm{d}l),$$

where

K = hydraulic conductivity (m/s),
A = the area of the sample (m^2),
$\mathrm{d}h$ = the difference in head across the sample (m), and
$\mathrm{d}l$ = the length of the sample (m).

The conductivity values were then converted to permeability (k, in square meters) using the following equation:

$$k = (K \times \mu)/(\rho \times g),$$

where

μ = viscosity (0.0008 Pa·s),
ρ = density (1020 kg/m^3), and
g = the gravitational constant (9.81 m/s^2).

The density value was estimated for a temperature of 30°C and a salinity of 33 kg/m^3, using the equation developed by Fofonoff (1985). Assuming a reasonable water compressibility, volume change, and thus density change due to the applied pressure, is minor (<0.1%). Viscosity data were obtained from the *Handbook of Chemistry and Physics* (Lide, 2000) for water at a temperature of 30°C and salinity of 35 kg/m^3. The

average permeability was computed as the arithmetic mean of permeability values at each effective stress. The maximum pressure change during testing was 0.83 MPa (120 psi).

Uncertainties due to variations during testing were examined by determining the standard deviation of flow rates and the pressure differences in the data used to calculate permeability. The variation in flow rate was estimated in terms of standard deviation for the highest and lowest flow rates used in this study. At the highest flow rate (1.44×10^{-3} mL/s), the estimated standard deviation was 2×10^{-5} mL/s, whereas at the lowest flow rate (1.17×10^{-6} mL/s), the estimated standard deviation was 2×10^{-8} mL/s. The variation in pressure difference was estimated using a representative sample, and the standard deviation varied from 0.00069 MPa at the lowest pressure difference (0.016 MPa) to 0.0012 at the highest pressure difference (0.069 MPa).

The corresponding porosity for each estimated permeability was calculated using the change in volume of fluid (mL) contained in the cell after each consolidation step. Total sample volume ($V_{T(0)}$) was calculated using $\pi r^2 h$, where r is the radius of the core sample and h is the height of the sample. Initial porosities (η_0) for volume calculations were obtained from D'Hondt, Jorgensen, Miller, et al. (2003). The estimated difference between the initial porosity (η_0) measurements and the porosity after backpressure is, on average, ~0.5% or less. Because the change in porosity is minor, we assumed that the porosity of the sample at the end of backpressure is similar to the initial porosity (η_0) of the sample.

Using the initial porosity (η_0), volume of voids before the testing ($V_{v(0)}$) was calculated:

$$V_{v(0)} = \eta_0 \times V_{T(0)}.$$

Volume of solids (V_s) was calculated using

$$V_s = V_{T(0)} - V_{v(0)}.$$

Using the difference of cell volumes between two consecutive steps (e.g., cell volume at backpressure and cell volume at first consolidation), the change in volume of water in the cell ($\Delta V_{T(1)}$) was calculated. The new total volume of the sample ($V_{T(1)}$) after pore spaces were reduced during the consolidation process was determined by subtracting the change in cell volume at the end of the consolidation step ($\Delta V_{T(1)}$) from the total sample volume ($V_{T(0)}$):

$$V_{T(1)} = V_{T(0)} - \Delta V_{T(1)}.$$

Using the calculated new total volume of the sample ($V_{T(1)}$), the new porosity at the end of the consolidation was calculated. The new porosity (η_1) at the end of the consolidation was

$$\eta_1 = (1 - V_s)/V_{T(1)}.$$

RESULTS

The samples represented depths ranging from 11 to 400 meters below seafloor from both the open-ocean and ocean-margin subsurface environments. Table T1 summarizes the measured permeability data for

T1. Permeability testing, p. 12.

each sample and the corresponding effective stress and porosity at each consolidation step. We applied four to five flow rates to each sample during the testing procedure to evaluate the repeatability of the measured permeabilities. The statistical errors for measured permeabilities have been quantified in terms of standard deviation as tabulated in Table T1. Our results indicate that the repeatability of permeability measurements is good. Permeabilities were measured at varying effective stress values ranging from 0.14 to 0.55 MPa. In general, permeabilities decreased with increasing effective stress (Fig. F4).

The measured permeabilities vary from ~8×10^{-19} m² to ~1×10^{-16} m². The lower permeabilities represent the lithified oozes and clay-rich sediments, whereas the higher permeabilities represent the unlithified oozes and silt-rich sediments. Site 1231 yielded the widest range of permeability values, varying from 1×10^{-16} m², representing carbonate-rich sediments deposited above the carbonate compensation depth (CCD), to 3×10^{-18} m², representing clay-rich sediments deposited below the CCD.

F4. Permeability response to increasing effective stress, p. 11.

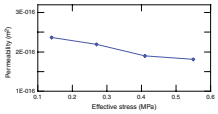

CONCLUSIONS

Eighteen core samples from ODP Leg 201 were used to measure vertical permeabilities of subsurface sediments from the equatorial Pacific and the Peru margin. Measured permeabilities ranged over three orders of magnitude from 10^{-18} m² to 10^{-16} m². The repeatability of measurements indicates that the error in the laboratory methods is small compared to the variation among sediment types. The lower permeabilities represent lithified oozes and clay-rich sediments, whereas the higher permeabilities represent unlithified oozes and silt-rich sediments. The rate of decrease in permeability with increasing effective stress varied among samples.

ACKNOWLEDGMENTS

This research used samples and data provided by the Ocean Drilling Program (ODP). ODP is sponsored by the U.S. National Science Foundation (NSF) and participating countries under management of Joint Oceanographic Institutions (JOI), Inc. Funding for this research was provided by JOI/U.S. Science Support Program postcruise grant. We thank Lizet Christiansen for helpful review of this manuscript.

REFERENCES

ASTM, 1990. Standard test method for measurement of hydraulic conductivity of saturated porous materials using a flexible wall permeameter. In *Annual Book of ASTM Standards:* Philadelphia (Am. Soc. Testing and Mater.), D5084-90:63–70.

Bolton, A., and Maltman, A., 1998. Fluid-flow pathways in actively deforming sediments: the role of pore fluid pressure and volume change. *Mar. Pet. Geol.,* 15:281–297.

Bolton, A., Maltman, A.J., and Fisher, Q., 2000. Anisotropic permeability and bimodal pore-size distributions of fine-grained marine sediments. *Mar. Pet. Geol.,* 17:657–672.

Chapelle, F., 1993. *Ground-Water Microbiology and Geochemistry:* New York (Wiley).

D'Hondt, S.L., Jørgensen, B.B., Miller, D.J., et al., 2003. *Proc. ODP, Init. Repts.,* 201 [Online]. Available from World Wide Web: <**http://www-odp.tamu.edu/publications/201_IR/201ir.htm**>. [Cited 2004-04-15]

Fofonoff, N.P., 1985. Physical properties of seawater: a new salinity scale and equation of state for seawater. *J. Geophys. Res.,* 90:3332–3342.

Lide, D.R. (Ed.), 2000. *Handbook of Chemistry and Physics:* Boca Raton, FL (Chemical Rubber Publishing Company).

Shipboard Scientific Party, 2003. Leg 201 summary. In D'Hondt, S.L., Jørgensen, B.B., Miller, D.J., et al., *Proc. ODP, Init. Repts.,* 201 [Online]. Available from World Wide Web: <**http://www-odp.tamu.edu/publications/201_IR/chap_01/chap_01.htm**>. [Cited 2004-04-15]

Figure F1. A. Map showing general locations of drill sites occupied during previous Legs (B) 138 and (C) 112. (Continued on next page.)

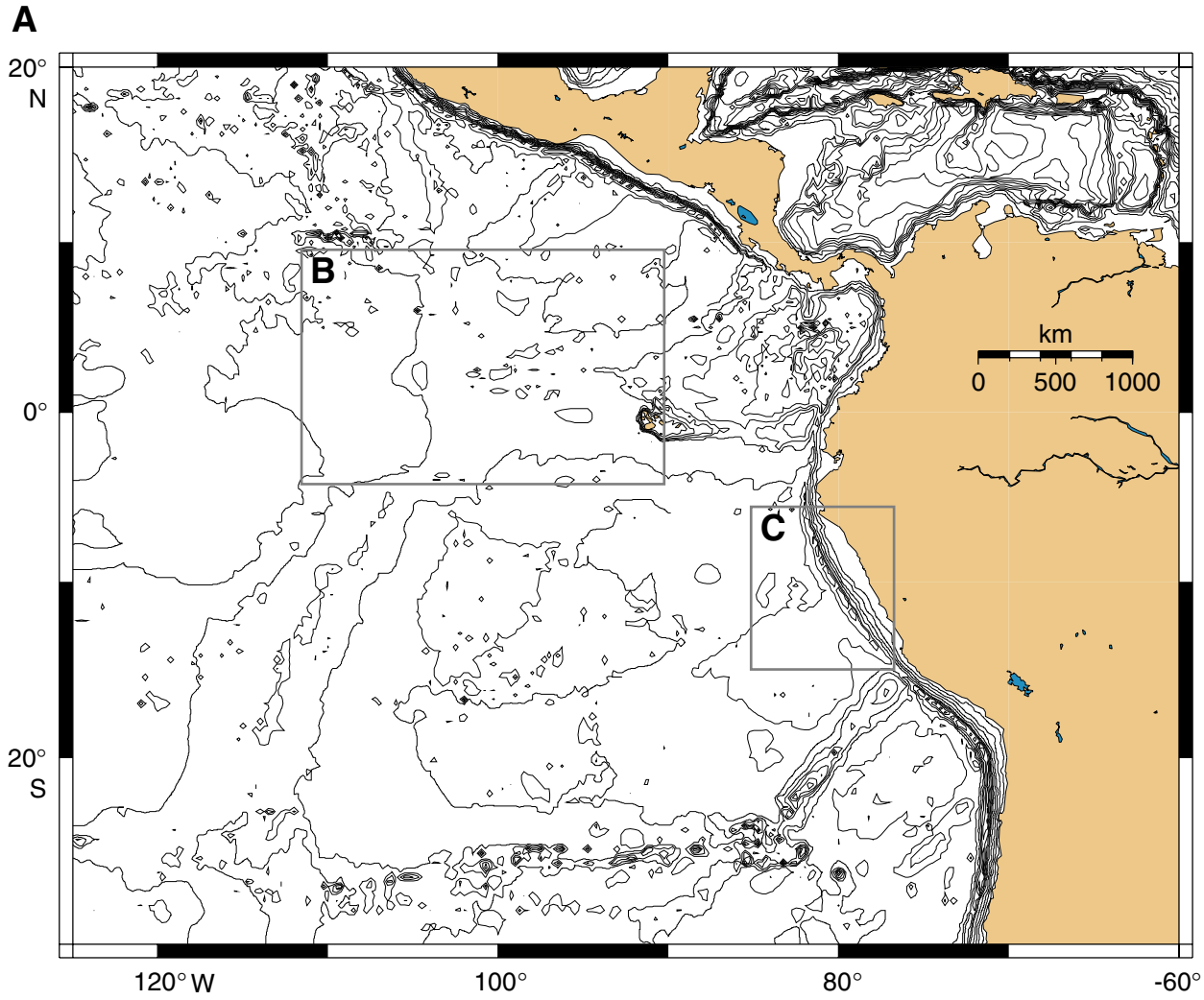

Figure F1 (continued). **B.** Location map of equatorial Pacific primary sites. Previous Ocean Drilling Program (ODP) site designations are in parentheses. **C.** Location map of Peru margin primary sites. Previous Deep Sea Drilling Project (DSDP)/ODP site designations are in parentheses (Shipboard Scientific Party, 2003).

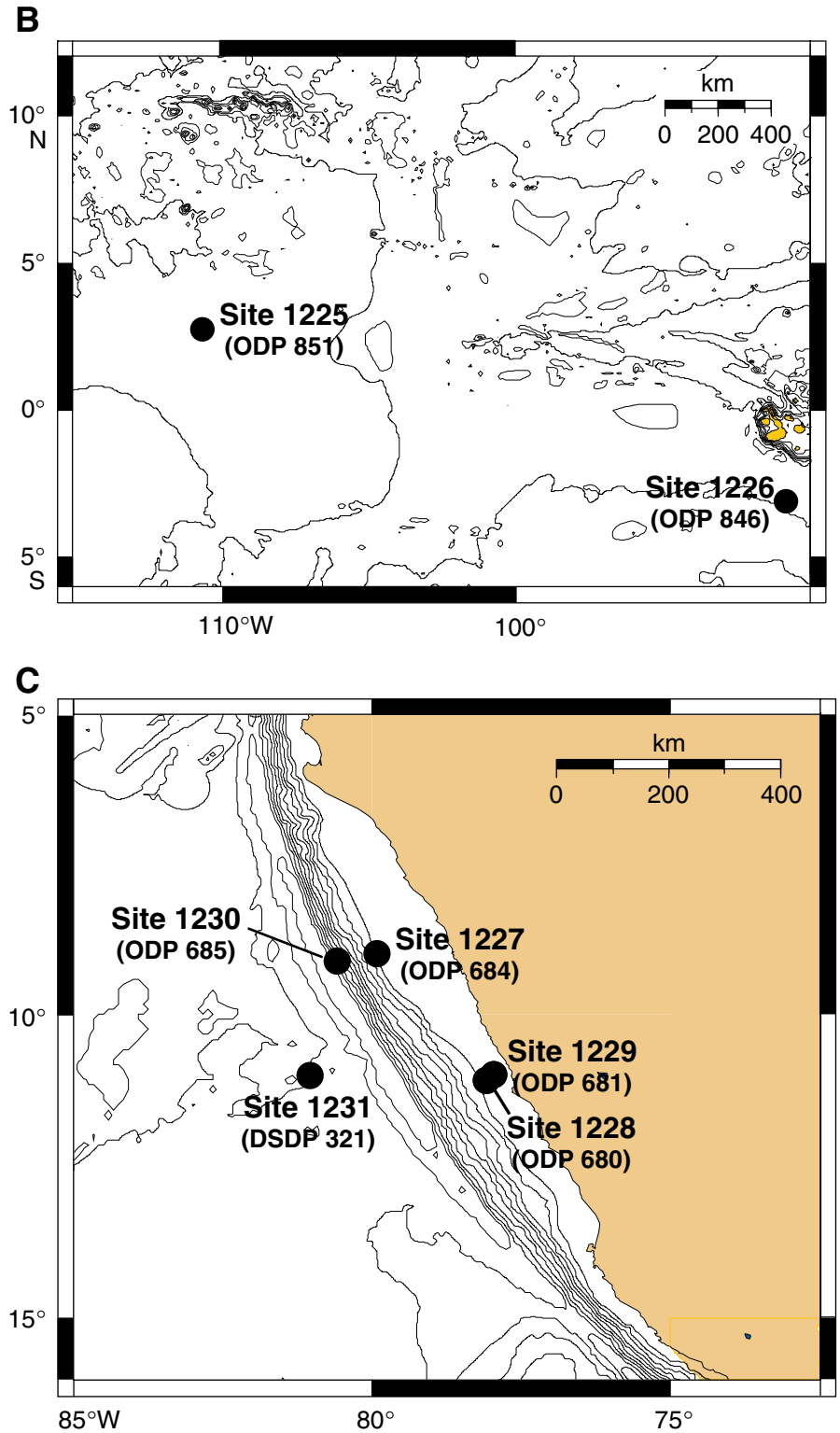

Figure F2. Laboratory setup for vertical permeability testing.

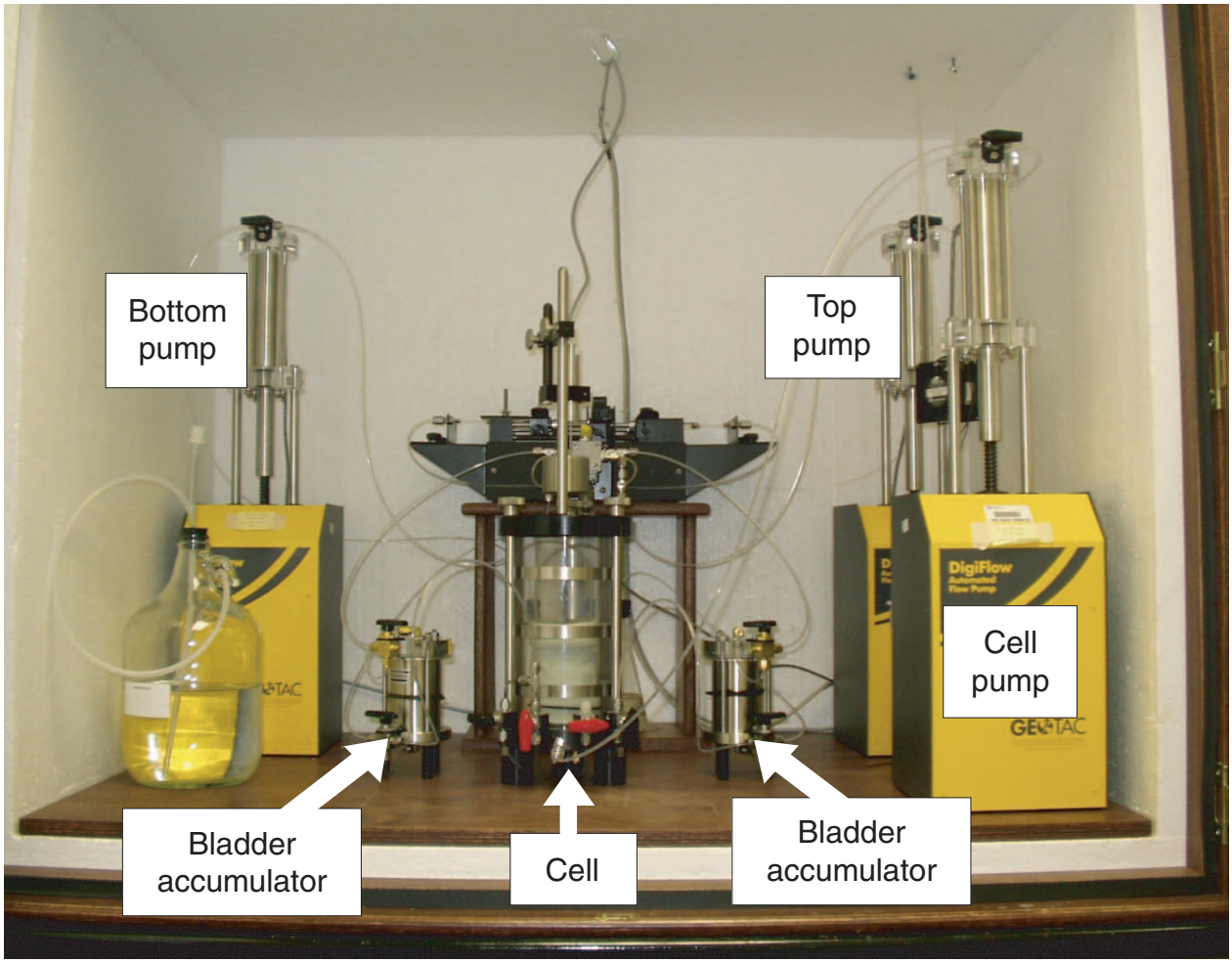

Figure F3. Constant-flow closed system used in permeability measurements. The permeameter cell is connected to the cell pump, which infuses and withdraws water at a constant rate of flow across the sample. The absolute pressure transducers measure the pressure difference across the sample (head change) and the pressure difference between the cell fluid and the pore water fluid (effective stress).

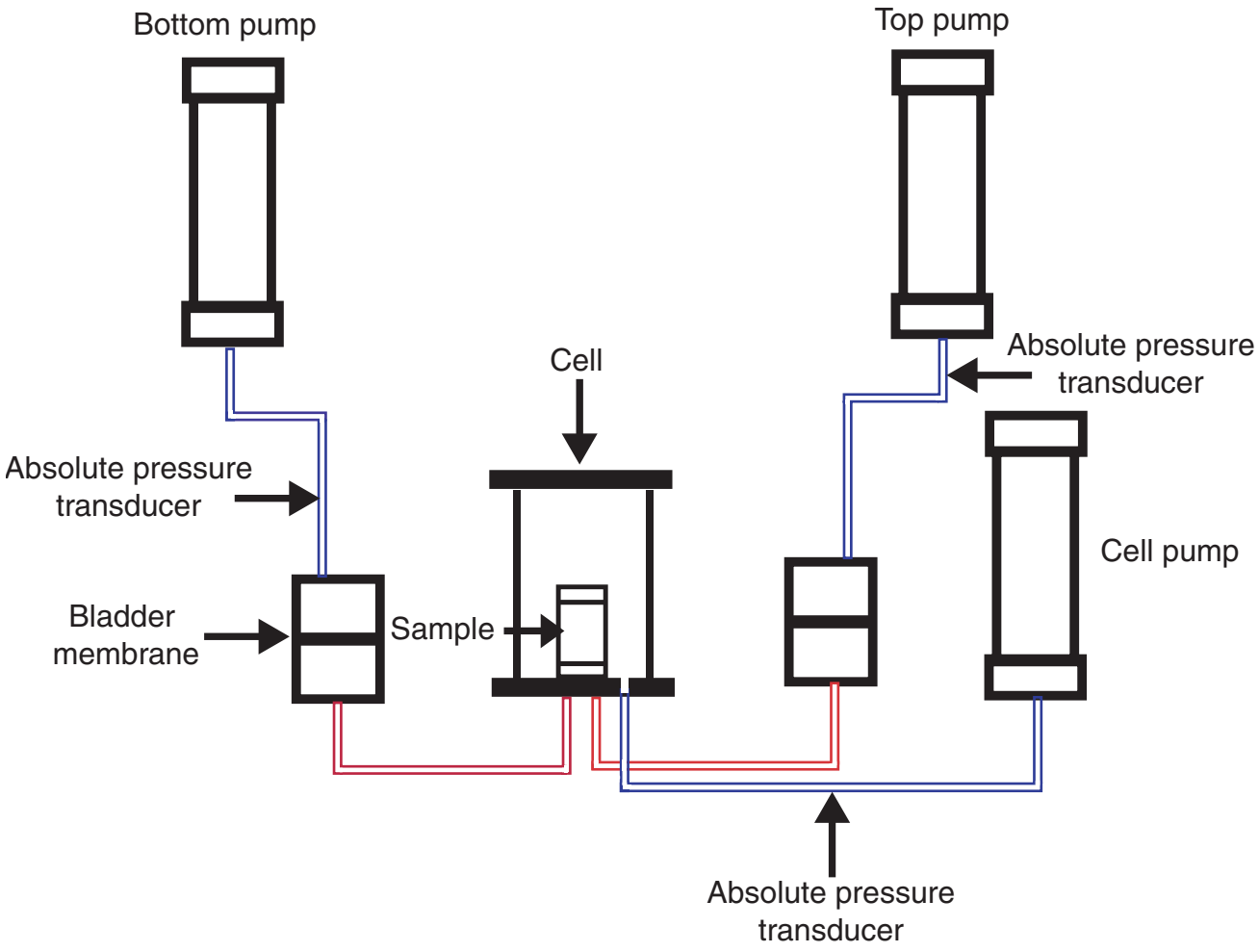

Figure F4. Permeability response to increasing effective stress for Section 201-1225A-34H-5.

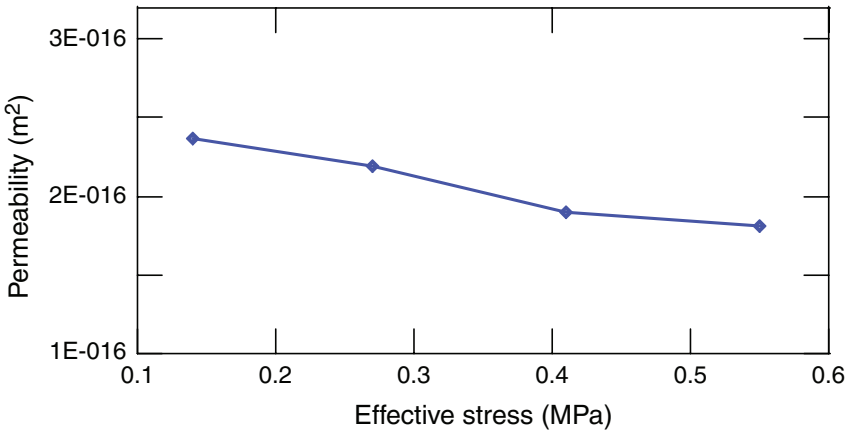

Table T1. Summary of permeability testing for samples from Leg 201, Sites 1225, 1226, 1227, 1230, and 1231. (See table note. Continued on next six pages.)

Core, section, interval (cm)	Depth (mbsf)	Description	Porosity (%)	Effective Stress (MPa)	Flow rate (mL/s) ($\times 10^{-5}$)	Permeability (m^2)	Standard deviation (m^2)
201-1225A-							
4H-1, 135–150	24.7	Carbonate and siliceous oozes and chalk	78.02	0.14	13.3	2.78×10^{-16}	
					15.0	4.07×10^{-16}	
					16.7	2.96×10^{-16}	
					25.0	5.00×10^{-16}	
					33.3	3.24×10^{-16}	
						3.61×10^{-16}	9.19×10^{-17}
			75.19	0.27	13.3	3.67×10^{-16}	
					15.0	1.77×10^{-16}	
					16.7	2.92×10^{-16}	
					25.0	2.72×10^{-16}	
					33.3	3.00×10^{-16}	
						2.82×10^{-16}	6.85×10^{-17}
			72.88	0.41	13.3	1.33×10^{-16}	
					15.0	1.77×10^{-16}	
					16.7	1.35×10^{-16}	
					25.0	2.28×10^{-16}	
					33.3	1.41×10^{-16}	
						1.63×10^{-16}	4.06×10^{-17}
			71.27	0.55	7.5	1.96×10^{-16}	
					10.0	2.61×10^{-16}	
					13.3	1.33×10^{-16}	
					15.0	1.29×10^{-16}	
					19.3	2.76×10^{-16}	
						1.99×10^{-16}	6.90×10^{-17}
201-1225A-							
10H-2, 135–150	83.2		68.30	0.14	10.0	2.46×10^{-16}	
					13.3	2.04×10^{-16}	
					16.7	2.10×10^{-16}	
					33.3	3.11×10^{-16}	
					50.0	2.33×10^{-16}	
						2.41×10^{-16}	4.30×10^{-17}
			65.63	0.27	10.0	2.43×10^{-16}	
					13.3	2.10×10^{-16}	
					16.7	2.09×10^{-16}	
					33.3	1.98×10^{-16}	
					50.0	1.97×10^{-16}	
						2.11×10^{-16}	1.87×10^{-17}
			64.76	0.41	10.0	1.55×10^{-16}	
					13.3	2.03×10^{-16}	
					16.7	1.59×10^{-16}	
					33.3	1.81×10^{-16}	
					50.0	1.48×10^{-16}	
						1.69×10^{-16}	2.25×10^{-17}
			63.82	0.55	10.0	1.61×10^{-16}	
					13.3	1.26×10^{-16}	
					16.7	1.50×10^{-16}	
					33.3	1.33×10^{-16}	
					50.0	1.41×10^{-16}	
						1.43×10^{-16}	1.37×10^{-17}
201-1225A-							
26H-6, 135–150	242.7		68.43	0.14	50.0	7.67×10^{-16}	
					58.3	7.25×10^{-16}	
					66.7	5.56×10^{-16}	
					75.0	7.14×10^{-16}	
					83.3	6.26×10^{-16}	
						6.78×10^{-16}	8.51×10^{-17}
			66.19	0.27	50.0	6.20×10^{-16}	
					58.3	5.65×10^{-16}	
					66.7	6.31×10^{-16}	
					75.0	5.62×10^{-16}	
					83.3	6.26×10^{-16}	
						6.01×10^{-16}	3.43×10^{-17}
			64.98	0.41	50.0	4.94×10^{-16}	
					58.3	6.10×10^{-16}	
					66.7	5.16×10^{-16}	
					75.0	5.28×10^{-16}	

Table T1 (continued).

Core, section, interval (cm)	Depth (mbsf)	Description	Porosity (%)	Effective Stress (MPa)	Flow rate (mL/s) ($\times 10^{-5}$)	Permeability (m^2)	Standard deviation (m^2)
					83.3	4.72×10^{-16}	
						$\mathbf{5.24 \times 10^{-16}}$	5.27×10^{-17}
			63.54	0.55	50.0	4.88×10^{-16}	
					58.3	4.31×10^{-16}	
					66.7	4.71×10^{-16}	
					75.0	4.25×10^{-16}	
					83.3	4.29×10^{-16}	
						$\mathbf{4.49 \times 10^{-16}}$	2.86×10^{-17}
201-1225A-							
34H-5, 0–15	309.7		64.04	0.14	13.3	2.07×10^{-16}	
					15.0	2.35×10^{-16}	
					25.0	2.37×10^{-16}	
					33.3	2.46×10^{-16}	
					41.7	2.61×10^{-16}	
						$\mathbf{2.37 \times 10^{-16}}$	1.97×10^{-17}
			62.68	0.27	13.3	2.34×10^{-16}	
					15.0	2.00×10^{-16}	
					25.0	2.24×10^{-16}	
					33.3	2.15×10^{-16}	
					41.7	2.22×10^{-16}	
						$\mathbf{2.19 \times 10^{-16}}$	1.24×10^{-17}
			61.72	0.41	13.3	1.70×10^{-16}	
					15.0	2.09×10^{-16}	
					25.0	1.80×10^{-16}	
					33.3	2.02×10^{-16}	
					41.7	1.91×10^{-16}	
						$\mathbf{1.90 \times 10^{-16}}$	1.59×10^{-17}
			61.05	0.55	13.3	1.51×10^{-16}	
					15.0	2.04×10^{-16}	
					25.0	1.79×10^{-16}	
					33.3	1.88×10^{-16}	
					41.7	1.86×10^{-16}	
						$\mathbf{1.81 \times 10^{-16}}$	1.94×10^{-17}
201-1226B-							
4H-1, 135–150	24.8	Carbonate and siliceous oozes and chalk	76.31	0.14	25.0	6.43×10^{-16}	
					33.3	7.41×10^{-16}	
					41.7	6.91×10^{-16}	
					50.0	7.33×10^{-16}	
					66.7	5.75×10^{-16}	
						$\mathbf{6.77 \times 10^{-16}}$	6.90×10^{-17}
			74.06	0.27	25.0	6.67×10^{-16}	
					33.3	4.74×10^{-16}	
					41.7	5.77×10^{-16}	
					50.0	4.63×10^{-16}	
					66.7	4.97×10^{-16}	
						$\mathbf{5.36 \times 10^{-16}}$	8.60×10^{-17}
			73.45	0.41	25.0	4.49×10^{-16}	
					33.3	4.82×10^{-16}	
					41.7	4.72×10^{-16}	
					50.0	4.85×10^{-16}	
					66.7	4.55×10^{-16}	
						$\mathbf{4.69 \times 10^{-16}}$	1.60×10^{-17}
			72.66	0.55	25.0	4.38×10^{-16}	
					33.3	4.22×10^{-16}	
					41.7	4.25×10^{-16}	
					50.0	4.10×10^{-16}	
					66.7	4.24×10^{-16}	
						$\mathbf{4.24 \times 10^{-16}}$	9.90×10^{-18}
201-1226B-							
26H-5, 115–130	239.6		67.32	0.14	28.4	2.88×10^{-16}	
					57.9	3.04×10^{-16}	
					77.9	3.11×10^{-16}	
					102.0	3.01×10^{-16}	
					144.0	3.12×10^{-16}	
						$\mathbf{3.04 \times 10^{-16}}$	9.67×10^{-18}
			66.83	0.27	31.7	2.87×10^{-16}	
					50.7	3.11×10^{-16}	
					88.7	3.11×10^{-16}	

Table T1 (continued).

Core, section, interval (cm)	Depth (mbsf)	Description	Porosity (%)	Effective Stress (MPa)	Flow rate (mL/s) ($\times 10^{-5}$)	Permeability (m^2)	Standard deviation (m^2)
					105.0	3.06×10^{-16}	
					149.0	3.18×10^{-16}	
						$\mathbf{3.06 \times 10^{-16}}$	1.17×10^{-17}
			66.09	0.41	20.5	2.84×10^{-16}	
					59.0	3.00×10^{-16}	
					84.3	2.92×10^{-16}	
					108.0	2.85×10^{-16}	
					128.0	2.97×10^{-16}	
						$\mathbf{2.92 \times 10^{-16}}$	6.82×10^{-18}
			65.40	0.55	34.4	3.17×10^{-16}	
					58.9	2.96×10^{-16}	
					68.9	2.74×10^{-16}	
					88.0	2.63×10^{-16}	
					130	2.78×10^{-16}	
						$\mathbf{2.86 \times 10^{-16}}$	2.12×10^{-17}
201-1226B-							
43X-1, 120–140	381.2		61.94	0.14	1.08	1.76×10^{-17}	
					1.17	1.51×10^{-17}	
					1.33	1.38×10^{-17}	
					1.50	1.51×10^{-17}	
					1.58	1.66×10^{-17}	
						$\mathbf{1.57 \times 10^{-17}}$	1.48×10^{-18}
			58.44	0.27	1.08	1.41×10^{-17}	
					1.17	1.32×10^{-17}	
					1.33	1.46×10^{-17}	
					1.50	1.26×10^{-17}	
					1.58	1.58×10^{-17}	
						$\mathbf{1.40 \times 10^{-17}}$	1.27×10^{-18}
			57.00	0.41	1.08	1.10×10^{-17}	
					1.17	1.38×10^{-17}	
					1.33	1.22×10^{-17}	
					1.50	1.33×10^{-17}	
					1.58	1.16×10^{-17}	
						$\mathbf{1.24 \times 10^{-17}}$	1.17×10^{-18}
			56.15	0.55	1.08	9.53×10^{-18}	
					1.17	1.02×10^{-17}	
					1.33	1.08×10^{-17}	
					1.50	1.03×10^{-17}	
					1.58	9.93×10^{-18}	
						$\mathbf{1.02 \times 10^{-17}}$	4.71×10^{-19}
201-1226B-							
46X-2, 110–130	409.4		57.51	0.14	0.117	2.22×10^{-18}	
					0.133	1.64×10^{-18}	
					0.150	2.38×10^{-18}	
					0.167	9.93×10^{-19}	
					0.250	2.02×10^{-18}	
						$\mathbf{1.85 \times 10^{-18}}$	5.52×10^{-19}
			55.62	0.27	0.117	1.04×10^{-18}	
					0.133	1.18×10^{-18}	
					0.150	1.80×10^{-18}	
					0.167	1.25×10^{-18}	
					0.250	1.76×10^{-18}	
						$\mathbf{1.41 \times 10^{-18}}$	3.51×10^{-19}
			53.43	0.41	0.117	1.04×10^{-18}	
					0.133	1.57×10^{-18}	
					0.150	1.05×10^{-18}	
					0.167	1.81×10^{-18}	
					0.250	1.18×10^{-18}	
						$\mathbf{1.33 \times 10^{-18}}$	3.45×10^{-19}
			52.02	0.55	0.117	8.10×10^{-19}	
					0.133	1.01×10^{-18}	
					0.150	2.30×10^{-18}	
					0.167	8.82×10^{-19}	
					0.250	1.26×10^{-18}	
						$\mathbf{1.25 \times 10^{-18}}$	6.09×10^{-19}

Table T1 (continued).

Core, section, interval (cm)	Depth (mbsf)	Description	Porosity (%)	Effective Stress (MPa)	Flow rate (mL/s) ($\times 10^{-5}$)	Permeability (m^2)	Standard deviation (m^2)
201-1227A-							
3H-3, 116–135	19.3	Organic-rich ocean-margin sediments	70.89	0.14	13.3	2.41×10^{-16}	
					14.2	2.42×10^{-16}	
					15.0	2.28×10^{-16}	
					15.8	2.60×10^{-16}	
					16.7	2.22×10^{-16}	
						2.39×10^{-16}	1.47×10^{-17}
			68.53	0.27	13.3	1.78×10^{-16}	
					14.2	1.73×10^{-16}	
					15.0	1.91×10^{-16}	
					15.8	1.74×10^{-16}	
					16.7	1.81×10^{-16}	
						1.79×10^{-16}	7.07×10^{-18}
			66.89	0.41	13.3	1.51×10^{-16}	
					14.2	1.52×10^{-16}	
					15.0	1.60×10^{-16}	
					15.8	1.45×10^{-16}	
					16.7	1.61×10^{-16}	
						1.54×10^{-16}	6.59×10^{-18}
			64.08	0.55	13.3	1.10×10^{-16}	
					14.2	1.16×10^{-16}	
					15.0	1.14×10^{-16}	
					15.8	1.14×10^{-16}	
					16.7	1.14×10^{-16}	
						1.13×10^{-16}	2.29×10^{-18}
201-1227A-							
12H-1, 130–150	101.9		70.46	0.14	8.33	1.86×10^{-16}	
					9.17	2.45×10^{-16}	
					10.0	2.51×10^{-16}	
					10.8	3.23×10^{-16}	
					11.7	2.27×10^{-16}	
						2.46×10^{-16}	4.99×10^{-17}
			68.07	0.27	8.33	2.17×10^{-16}	
					9.17	1.49×10^{-16}	
					10.0	2.07×10^{-16}	
					10.8	1.33×10^{-16}	
					11.7	1.95×10^{-16}	
						1.80×10^{-16}	3.72×10^{-17}
			67.3	0.41	8.33	1.44×10^{-16}	
					9.17	1.94×10^{-16}	
					10.0	1.55×10^{-16}	
					10.8	1.69×10^{-16}	
					11.7	1.38×10^{-16}	
						1.60×10^{-16}	2.23×10^{-17}
			66.32	0.55	8.33	1.57×10^{-16}	
					9.17	1.43×10^{-16}	
					10.0	7.36×10^{-17}	
					10.8	8.03×10^{-17}	
					11.7	7.14×10^{-17}	
						1.05×10^{-16}	4.13×10^{-17}
201-1230A-							
4H-5, 117–135	31.0	Clay-rich diatomaceous mud and diatom ooze	68.45	0.14	0.667	1.18×10^{-17}	
					1.00	2.74×10^{-17}	
					1.33	1.99×10^{-17}	
					1.67	1.59×10^{-17}	
					3.33	1.76×10^{-17}	
						1.85×10^{-17}	5.77×10^{-18}
			67.32	0.27	0.667	1.76×10^{-17}	
					1.00	1.66×10^{-17}	
					1.33	2.19×10^{-17}	
					1.67	1.45×10^{-17}	
					3.33	1.45×10^{-17}	
						1.70×10^{-17}	3.04×10^{-18}
			65.63	0.41	0.667	1.23×10^{-17}	
					1.00	1.41×10^{-17}	
					1.33	1.52×10^{-17}	
					1.67	1.23×10^{-17}	
					3.33	1.13×10^{-17}	

Table T1 (continued).

Core, section, interval (cm)	Depth (mbsf)	Description	Porosity (%)	Effective Stress (MPa)	Flow rate (mL/s) (× 10^{-5})	Permeability (m^2)	Standard deviation (m^2)
						1.30×10^{-17}	1.56×10^{-18}
			64.41	0.55	0.667	1.87×10^{-17}	
					1.00	9.22×10^{-18}	
					1.33	1.22×10^{-17}	
					1.67	8.42×10^{-18}	
					3.33	8.90×10^{-18}	
						1.15×10^{-17}	4.28×10^{-18}
201-1230A-							
9H-8, 78–98	70.7		68.31	0.14	1.67	6.58×10^{-17}	
					3.33	5.55×10^{-17}	
					5.00	6.24×10^{-17}	
					6.67	5.73×10^{-17}	
					8.33	4.66×10^{-17}	
						5.75×10^{-17}	7.35×10^{-18}
			68.04	0.27	1.67	4.25×10^{-17}	
					3.33	4.50×10^{-17}	
					5.00	4.31×10^{-17}	
					6.67	3.94×10^{-17}	
					8.33	4.22×10^{-17}	
						4.24×10^{-17}	2.01×10^{-18}
			67.43	0.41	1.67	3.84×10^{-17}	
					3.33	3.23×10^{-17}	
					5.00	3.52×10^{-17}	
					6.67	3.34×10^{-17}	
					8.33	3.04×10^{-17}	
						3.39×10^{-17}	3.05×10^{-18}
			66.91	0.55	1.67	2.97×10^{-17}	
					3.33	3.54×10^{-17}	
					5.00	3.03×10^{-17}	
					6.67	3.13×10^{-17}	
					8.33	2.77×10^{-17}	
						3.09×10^{-17}	2.82×10^{-18}
201-1230A-							
31X-1, 115–135	230.8		52.87	0.14	1.33	3.48×10^{-17}	
					1.50	4.20×10^{-17}	
					1.67	2.82×10^{-17}	
					3.33	3.27×10^{-17}	
					5.00	2.85×10^{-17}	
						3.32×10^{-17}	5.65×10^{-18}
			49.48	0.27	1.33	2.30×10^{-17}	
					1.50	1.73×10^{-17}	
					1.67	2.03×10^{-17}	
					3.33	1.87×10^{-17}	
					5.00	1.79×10^{-17}	
						1.94×10^{-17}	2.28×10^{-18}
			47.70	0.41	1.33	2.09×10^{-17}	
					1.50	1.90×10^{-17}	
					1.67	1.44×10^{-17}	
					3.33	1.61×10^{-17}	
					5.00	1.10×10^{-17}	
						1.63×10^{-17}	3.86×10^{-18}
			45.43	0.55	1.33	1.45×10^{-17}	
					1.50	2.16×10^{-17}	
					1.67	1.08×10^{-17}	
					3.33	1.37×10^{-17}	
					5.00	1.26×10^{-17}	
						1.47×10^{-17}	4.13×10^{-18}
201-1230A-							
35X-6, 0–20	252.1		58.37	0.14	0.833	1.98×10^{-17}	
					1.00	2.15×10^{-17}	
					1.17	1.95×10^{-17}	
					1.33	1.93×10^{-17}	
					1.50	2.07×10^{-17}	
						2.02×10^{-17}	9.44×10^{-19}
			54.91	0.27	0.833	2.17×10^{-17}	
					1.00	2.48×10^{-17}	
					1.17	1.30×10^{-17}	
					1.33	1.57×10^{-17}	

Table T1 (continued).

Core, section, interval (cm)	Depth (mbsf)	Description	Porosity (%)	Effective Stress (MPa)	Flow rate (mL/s) ($\times 10^{-5}$)	Permeability (m^2)	Standard deviation (m^2)
					1.50	1.42×10^{-17}	
						1.79×10^{-17}	5.09×10^{-18}
			52.97	0.41	0.833	1.55×10^{-17}	
					1.00	1.64×10^{-17}	
					1.17	1.38×10^{-17}	
					1.33	1.11×10^{-17}	
					1.50	1.35×10^{-17}	
						1.41×10^{-17}	2.02×10^{-18}
			51.42	0.55	0.833	1.48×10^{-17}	
					1.00	1.03×10^{-17}	
					1.17	1.68×10^{-17}	
					1.33	1.14×10^{-17}	
					1.50	8.90×10^{-18}	
						1.25×10^{-17}	3.27×10^{-18}
201-1231B-							
3H-3, 115–135	17.1	Clay and nannofossil ooze	89.05	0.14	1.33	4.23×10^{-17}	
					1.50	2.73×10^{-17}	
					1.67	3.08×10^{-17}	
					3.33	2.84×10^{-17}	
					5.00	2.80×10^{-17}	
						3.14×10^{-17}	6.23×10^{-18}
			86.80	0.27	1.33	1.16×10^{-17}	
					1.50	1.10×10^{-17}	
					1.67	9.53×10^{-18}	
					3.33	9.22×10^{-18}	
					5.00	9.46×10^{-18}	
						1.02×10^{-17}	1.08×10^{-18}
			86.00	0.41	1.33	6.38×10^{-18}	
					1.50	7.09×10^{-18}	
					1.67	6.77×10^{-18}	
					3.33	6.86×10^{-18}	
					5.00	6.75×10^{-18}	
						6.77×10^{-18}	2.56×10^{-19}
			84.69	0.55	1.33	2.99×10^{-18}	
					1.50	3.05×10^{-18}	
					1.67	3.13×10^{-18}	
					3.33	4.58×10^{-18}	
						3.44×10^{-18}	7.62×10^{-19}
201-1231B-							
6H-2, 124–150	44.1		84.74	0.14	6.67	1.87×10^{-16}	
					8.33	1.48×10^{-16}	
					10.0	1.34×10^{-16}	
					11.7	1.41×10^{-16}	
					13.3	1.36×10^{-16}	
						1.49×10^{-16}	2.17×10^{-17}
			83.48	0.27	6.67	5.46×10^{-17}	
					8.33	5.02×10^{-17}	
					10.0	5.02×10^{-17}	
					11.7	5.47×10^{-17}	
					13.3	5.82×10^{-17}	
						5.36×10^{-17}	3.42×10^{-18}
			81.88	0.41	6.7	2.50×10^{-17}	
					8.3	2.34×10^{-17}	
					10.0	2.61×10^{-17}	
					11.7	2.49×10^{-17}	
					13.3	2.49×10^{-17}	
						2.49×10^{-17}	9.36×10^{-19}
			80.05	0.55	6.7	1.46×10^{-17}	
					8.3	1.41×10^{-17}	
					10.0	1.41×10^{-17}	
					11.7	1.53×10^{-17}	
					13.3	1.75×10^{-17}	
						1.51×10^{-17}	1.39×10^{-18}

Table T1 (continued).

Core, section, interval (cm)	Depth (mbsf)	Description	Porosity (%)	Effective Stress (MPa)	Flow rate (mL/s) ($\times 10^{-5}$)	Permeability (m^2)	Standard deviation (m^2)
201-1231B-							
9H-4, 130–150	75.7		59.42	0.14	50.0	9.38×10^{-16}	
					58.3	6.38×10^{-16}	
					66.7	8.90×10^{-16}	
					75.0	6.31×10^{-16}	
					83.3	7.79×10^{-16}	
						7.75×10^{-16}	1.41×10^{-16}
			58.02	0.27	50.0	5.23×10^{-16}	
					58.3	6.27×10^{-16}	
					66.7	5.80×10^{-16}	
					75.0	5.78×10^{-16}	
					83.3	5.20×10^{-16}	
						5.66×10^{-16}	4.47×10^{-17}
			57.39	0.41	50.0	4.37×10^{-16}	
					58.3	4.85×10^{-16}	
					66.7	4.32×10^{-16}	
					75.0	4.85×10^{-16}	
					83.3	4.37×10^{-16}	
						4.55×10^{-16}	2.71×10^{-17}
			56.45	0.55	50.0	4.45×10^{-16}	
					58.3	4.12×10^{-16}	
					66.7	4.41×10^{-16}	
					75.0	4.15×10^{-16}	
					83.3	4.16×10^{-16}	
						4.26×10^{-16}	1.59×10^{-17}
201-1231B-							
13H-2, 115–135	112.1		66.02	0.14	13.30	5.09×10^{-16}	
					16.7	4.27×10^{-16}	
					20	4.37×10^{-16}	
					23.3	5.09×10^{-16}	
					26.7	4.32×10^{-16}	
						4.63×10^{-16}	4.23×10^{-17}
			64.57	0.27	13.30	3.42×10^{-16}	
					16.7	4.57×10^{-16}	
					20	3.92×10^{-16}	
					23.3	4.35×10^{-16}	
						4.17×10^{-16}	
						4.09×10^{-16}	4.41×10^{-17}
			63.59	0.41	13.30	3.84×10^{-16}	
					16.7	3.76×10^{-16}	
					20	3.62×10^{-16}	
					23.3	4.02×10^{-16}	
					26.7	3.68×10^{-16}	
						3.78×10^{-16}	1.57×10^{-17}
			62.86	0.55	13.30	4.32×10^{-16}	
					16.7	3.07×10^{-16}	
					20	3.93×10^{-16}	
					23.3	3.10×10^{-16}	
					26.7	3.87×10^{-16}	
						3.66×10^{-16}	5.52×10^{-17}

Note: The linear average permeability values for each of the four runs are given in bold.